Correlation Effects in Quantum Spin-Hall Insulators: A Quantum Monte Carlo Study

M. Hohenadler, T. C. Lang, and F. F. Assaad

Institut für Theoretische Physik und Astrophysik, Universität Würzburg, Am Hubland, 97074 Würzburg, Germany

(Received 29 November 2010; revised manuscript received 3 February 2011; published 7 March 2011)

We consider the Kane-Mele model supplemented by a Hubbard U term. The phase diagram is mapped out using projective auxiliary field quantum Monte Carlo simulations. The quantum spin liquid of the Hubbard model is robust against weak spin-orbit interaction, and is not adiabatically connected to the spin-Hall insulating state. Beyond a critical value of $U > U_c$ both states are unstable toward magnetic ordering. In the quantum spin-Hall state we study the spin, charge, and single-particle dynamics of the helical Luttinger liquid by retaining the Hubbard interaction only on a ribbon edge. The Hubbard interaction greatly suppresses charge currents along the edge and promotes edge magnetism but leaves the single-particle signatures of the helical liquid intact.

DOI: 10.1103/PhysRevLett.106.100403 PACS numbers: 75.10.−b, 03.65.Vf, 71.10.Pm, 71.30.+h

The Z_2 topological band insulator (TBI) [1] arises from spin-orbit (SO) coupling and is invariant under time reversal symmetry. The bulk is insulating and the edge states, coined helical Luttinger liquids, show gapless spin and charge excitations. An explicit realization is given by the Kane-Mele (KM) Hamiltonian [2], which reduces to two separate Haldane models [3], with opposite signs of the Hall conductivity in the two spin sectors. Time reversal symmetry protects the edge states against potential scattering and weak electron-electron interactions [4,5], and allows for experimental realizations [6,7]. Previous work on correlation effects has essentially followed two routes: interaction driven topological insulators [8–12] or (as here) the interplay of spin-orbit coupling and Coulomb repulsion [13–17]. We present the first quantum Monte Carlo (QMC) results which document (i) a quantum phase transition between the quantum spin liquid (QSL) phase of [18] and the TBI, (ii) the stability of the TBI against magnetic ordering, and (iii) the role of fluctuations in the helical edge states of the TBI.

Our starting point is the KM-Hubbard model on the honeycomb lattice with Hamiltonian $H = H_{\mathrm{KM}} + H_U$,

$$H_{\mathrm{KM}} = -t\sum_{\langle \mathbf{i},\mathbf{j}\rangle} c_{\mathbf{i}}^{\dagger} c_{\mathbf{j}} + i\lambda \sum_{\langle\langle \mathbf{i},\mathbf{j}\rangle\rangle} c_{\mathbf{i}}^{\dagger}\mathbf{e}_{\mathbf{i},\mathbf{j}}\cdot\boldsymbol{\sigma} c_{\mathbf{j}},$$
$$H_U = \frac{U}{2}\sum_{\mathbf{i}} (c_{\mathbf{i}}^{\dagger} c_{\mathbf{i}} - 1)^2. \tag{1}$$

The spinor $c_{\mathbf{i}}^{\dagger} = (c_{\mathbf{i},\uparrow}^{\dagger}, c_{\mathbf{i},\downarrow}^{\dagger})$ creates an electron in a Wannier state at site $\mathbf{i}$, $\langle \mathbf{i}, \mathbf{j}\rangle$ means summation over the three nearest neighbors $\mathbf{j} = \mathbf{i} + \boldsymbol{\delta}_n$ with $\boldsymbol{\delta}_n \in \{\pm\boldsymbol{\delta}_1, \pm\boldsymbol{\delta}_2, \pm\boldsymbol{\delta}_3\}$, see Fig. 1(a), $\langle\langle \mathbf{i}, \mathbf{j}\rangle\rangle$ denotes summation over next-nearest neighbors $\mathbf{j} = \mathbf{i} + \boldsymbol{\delta}_n + \boldsymbol{\delta}_m$, $\mathbf{e}_{\mathbf{i},\mathbf{j}} = \boldsymbol{\delta}_n \times \boldsymbol{\delta}_m/|\boldsymbol{\delta}_n \times \boldsymbol{\delta}_m|$ and $\boldsymbol{\sigma}$ is the vector of Pauli matrices. At the particle-hole symmetric point, this model can be investigated with a variety of QMC algorithms without encountering the infamous negative sign problem. We present two sets of simulations to extract bulk and boundary properties.

Bulk phase diagram.—For bulk simulations we use the projective auxiliary field QMC approach. The ground state $|\Psi_0\rangle$ is filtered out of a trial wave function $|\Psi_{\mathrm{T}}\rangle$ with $\langle\Psi_{\mathrm{T}}|\Psi_0\rangle \neq 0$; a very good choice is the ground state of the KM model. For an arbitrary observable, $\langle\Psi_0|O|\Psi_0\rangle = \lim_{\Theta\to\infty}\langle\Psi_{\mathrm{T}}|e^{-\Theta H/2} O e^{-\Theta H/2}|\Psi_{\mathrm{T}}\rangle/\langle\Psi_{\mathrm{T}}|e^{-\Theta H}|\Psi_{\mathrm{T}}\rangle$. The absence of the negative sign problem at half filling follows from the fact that, after a discrete Hubbard-Stratonovich transformation of H_U and subsequent integration over the fermionic degrees of freedom, the fermionic determinants in the up and down spin sectors are linked via complex conjugation such that their product is positive. We employ an $SU(2)$ invariant Hubbard-Stratonovich transformation and an imaginary time discretization of $\Delta\tau t = 0.1$. Projection parameters $\Theta t = 40$ prove sufficient for converged (within statistical errors) ground-state results. For details of the algorithm, see [19].

The SO coupling reduces the $SU(2)$ symmetry to a $U(1)$ symmetry corresponding to spin rotations around the z axis. The Hubbard interaction promotes transverse, x-y magnetic ordering [15] which can be tracked by

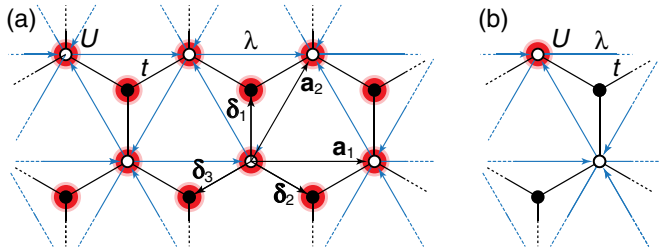

FIG. 1 (color online). (a) Periodic lattice structure of the KM-Hubbard model with nearest-neighbor hopping t, spin-orbit coupling λ, and Coulomb repulsion U. Arrows indicate the current direction associated with the spin-orbit term for one spin species and sublattice. (b) Effective model on a semi-infinite ribbon with periodic boundaries in the $\mathbf{a}_1$ direction and Coulomb repulsion U only at the edge sites.

computing the transverse antiferromagnetic (AFM) structure factor

$$S^{xy}_{\mathrm{AFM}} = \frac{1}{L^2}\sum_{\mathbf{i},\mathbf{j}}(-1)^{\mathbf{i}+\mathbf{j}}\langle\Psi_0|S^+_{\mathbf{i}}S^-_{\mathbf{j}} + S^-_{\mathbf{i}}S^+_{\mathbf{j}}|\Psi_0\rangle, \qquad (2)$$

on $L \times L$ honeycomb lattices with periodic boundary conditions. At $\lambda/t = 0.25$, this quantity is plotted versus lattice size for various values of U/t in the inset of Fig. 2. The onset of long-range order occurs in the region $6 < U_c/t < 6.25$. Because of the underlying $U(1)$ symmetry, the quantum phase transition between the magnetically ordered and disordered phases is expected to be in the 3D-XY universality class. Figure 2 shows U_c/t as a function of λ/t and thus defines the magnetic phase diagram.

Several aspects of Fig. 2 deserve comments. (i) With the important exception of the QSL phase, the qualitative aspects of the magnetic phase diagram were obtained at the mean-field level [15]. The magnetic instability smoothly converges to the $\lambda/t = 0$ result [18]. For $0.025 < \lambda/t < 0.25$ we observe no spin ordering along the z quantization axis up to $U/t = 9$. (ii) The $U/t = 0$ line corresponds to the KM model and describes a TBI with a single-particle gap set by λ. (iii) The $\lambda/t = 0$ line has been investigated in detail in Ref. [18]. Up to $U/t = 3.5$ the semimetallic (SM) phase remains stable, and magnetic order sets in from $U/t = 4.3$ onwards. The intermediate phase shows both spin and single-particle gaps and corresponds to a QSL.

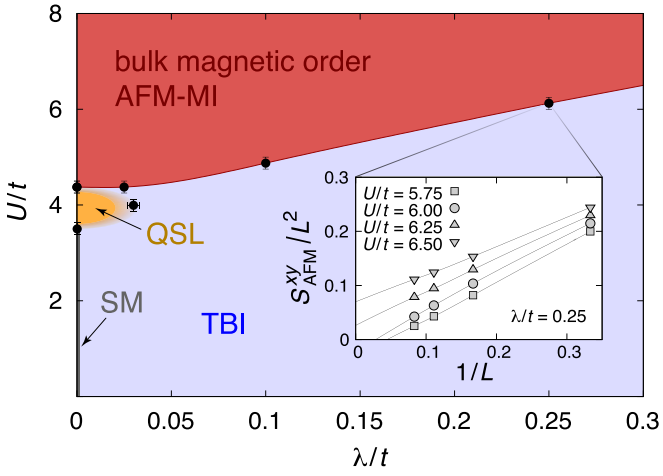

FIG. 2 (color online). Phase diagram of the KM-Hubbard model from QMC simulations. Bullets correspond to computed phase boundaries. The four phases are the semimetal (SM), the quantum spin liquid (QSL), the topological or quantum spin-Hall insulator (TBI), and the antiferromagnetic Mott insulator (AFM-MI). Inset: Ground-state spin-spin correlation function [Eq. (2)] for an $L \times L$ honeycomb lattice with periodic boundary conditions and $\lambda/t = 0.25$. Lines are fits to the form $a + b/L + c/L^2$. Negative values indicate that the data decay quicker than $1/L^2$. Here and in subsequent figures, error bars are omitted if smaller than the symbol size.

To further investigate the phase diagram and, in particular, the evolution of the QSL upon switching on the SO coupling, we have computed the single-particle gap Δ_{sp} at the Dirac point $\mathbf{K}$. This quantity is extracted by fitting the tail of the single-particle imaginary time Green function, $G(\mathbf{K},\tau) = \langle\Psi_0|c^\dagger_{\mathbf{K},\sigma}(\tau)c_{\mathbf{K},\sigma}|\Psi_0\rangle$ [see Fig. 3(c)], to the form $Ze^{-\tau\Delta_{\mathrm{sp}}}$, where Z corresponds to the quasiparticle residue. The extrapolated (in L) value of Δ_{sp} is plotted in Figs. 3(a) and 3(b) along different cuts of the phase diagram. Starting in the SM phase, at $U/t = 2$, $\Delta_{\mathrm{sp}} \propto \lambda$ as for the $U/t = 0$ case and characteristic of the TBI state [2]. In contrast, in the QSL phase at $U/t = 4$, Δ_{sp} initially decreases with increasing λ but grows again for $\lambda/t \gtrsim 0.03$. We interpret this cusp feature as a signature of a quantum phase transition between the QSL state and the TBI at $\lambda_c/t \simeq 0.03$. The data support the vanishing of the single-particle gap at λ_c/t [20]. Figure 3(b) shows that the magnetic transition as a function of U/t at fixed $\lambda/t = 0.1$ is equally apparent; Δ_{sp} smoothly evolves from its $U/t = 0$ value and exhibits a cusp feature at $U_c/t \simeq 4.9$. Magnetic order breaks time reversal symmetry and lifts the topological protection, so that Δ_{sp} does not have to close at U_c. This evolution of the gap can be qualitatively reproduced at the mean-field level. From the single-particle gap, we identify four distinct phases: (i) a TBI phase, where Δ_{sp} evolves smoothly to its $U/t = 0$ value, (ii) a magnetically ordered MI, (iii) a SM line, and (iv) a QSL phase.

Edge states in the TBI phase.—Edge states are a hallmark feature of TBIs. A detailed understanding of correlation effects in these one-dimensional liquids is crucial

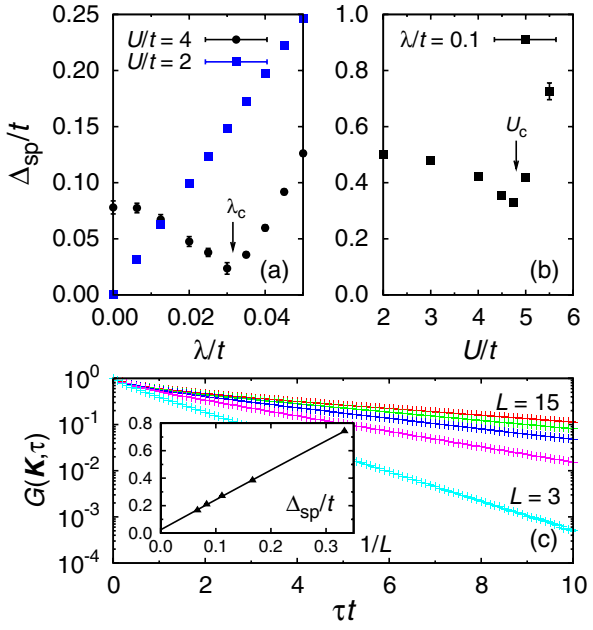

FIG. 3 (color online). (a),(b) Single-particle gap along different cuts in Fig. 2 ($\lambda_c/t \simeq 0.03$, $U_c/t \simeq 4.9$). (c) Raw data and size extrapolation (inset) at $U/t = 4$, $\lambda/t = 0.03$.

for theory and experiment. To study the helical Luttinger liquid formed at the edge of the Z_2 TBI, we consider the ribbon topology of Fig. 1(b). For $U \geq U_c$, time reversal symmetry is broken spontaneously, and scattering between the left spin-down and right spin-up movers of the helical liquid is allowed, thus opening a gap in the edge states and destroying the TBI state. As argued above, at $U < U_c$ the bulk is adiabatically linked to the $U/t = 0$ line. Since furthermore the helical liquid is exponentially localized on the boundary (as readily seen in the KM model), we retain the Hubbard interaction only on one zigzag edge of the ribbon [cf. Fig. 1(b)]. With this ansatz, the bulk plays the role of a fermionic bath which can be integrated out at the expense of a Gaussian integral. This yields an effective one-dimensional action,

$$\mathcal{S} = -\sum_{\sigma,r,r'} \int_0^\beta d\tau \int_0^\beta d\tau' c^\dagger_{r,\sigma} G^{-1}_{0,\sigma}(r-r') c_{r',\sigma} + U \sum_r \int_0^\beta \left[n_{r,\uparrow}(\tau) - \frac{1}{2} \right] \left[n_{r,\downarrow}(\tau) - \frac{1}{2} \right], \quad (3)$$

where r is an edge site index and $G_{0,\sigma}(r-r')$ is the free Green function of the KM model on the ribbon topology. We can solve the action (3) exactly using the weak-coupling expansion continuous-time QMC method [21,22], on arbitrarily wide $L \times L'$ ribbons (here $L' = 64$). The validity of this effective model at $U < U_c$ has been verified by QMC simulations for the full model (1) on narrow ribbons. We take $\lambda/t = 0.25$ in the following.

At $U/t = 0$ and half filling, the dispersion relation of the helical liquid satisfies $\varepsilon_{q,\uparrow} = -\varepsilon_{q,\downarrow}$, and the edge states are unstable towards transverse *ferromagnetic* order. Figure 4 shows the development of substantial spin-spin correlations in the transverse direction with decreasing temperature and increasing U/t. This corresponds to the dominant correlation function.

We calculate dynamic structure factors along the edge,

$$O(q,\omega) = \frac{1}{Z} \sum_{n,m} e^{-\beta E_n} |\langle m|O(q)|n\rangle|^2 \delta(E_m - E_0 - \omega). \quad (4)$$

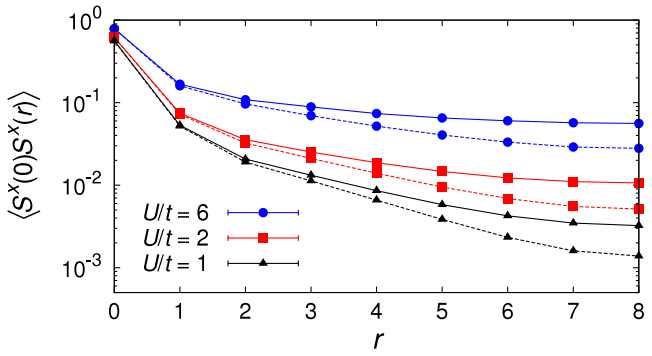

FIG. 4 (color online). Transverse spin correlations along the edge of the ribbon. Results are for $L = 16$, $\beta t = 20$ (dashed lines) and $\beta t = 40$ (solid lines). Lines are guides to the eye.

For charge, $N(q,\omega)$, $O(q) = N(q) = \frac{1}{\sqrt{L}} \sum_r e^{iqr} n_r$, and for spin, $S^\alpha(q,\omega)$, $O(q) = S^\alpha(q) = \frac{1}{\sqrt{L}} \sum_r e^{iqr} S^\alpha_r$. Single-particle dynamics are deduced from the single-particle Green function via the spectral functions $A_\sigma(q,\omega) = -\pi^{-1} \mathrm{Im} G_\sigma(q,\omega)$, where by time reversal symmetry we have $A_\uparrow(q,\omega) = A_\downarrow(-q,\omega)$.

Figure 5 shows these dynamic quantities at $U/t = 2$. The dominant features of the single-particle spectral function, see Fig. 5(b), follow the noninteracting system: within the bulk band gap, gapless single-particle excitations emerge with a velocity tied to the z component of the spin. For $U/t = 0$, the particle-hole spectra can be deduced from the single-particle dynamics by computing the bubble. Within this framework the dynamic charge structure factor as well as the z component of the dynamic spin structure factor are identical. Both quantities conserve the z component of spin, such that at low energies (i.e., below the bulk gap) only particle-hole excitations within the left or right movers are allowed. This produces a linear mode around $q = 0$ as observed in Figs. 5(a) and 5(d). At higher energies, particle-hole excitations involving bulk states become apparent. Upon inspection of Figs. 5(a) and 5(d) one sees that the support of both quantities is very similar. However, the spectral weight of the low-lying charge modes is greatly suppressed in comparison to the longitudinal spin mode. The transverse spin susceptibility involves a spin-flip process and hence excitations between the left and right dispersion relations. This produces a continuum of excitations in the long-wavelength limit [cf. Fig. 5(c)].

At large $U/t = 5$ (Fig. 6) we observe a strong depletion of spectral weight in the low-lying charge modes [Fig. 6(a)], which leads to reduction of the Drude weight by 1 order of magnitude. In contrast, despite strong

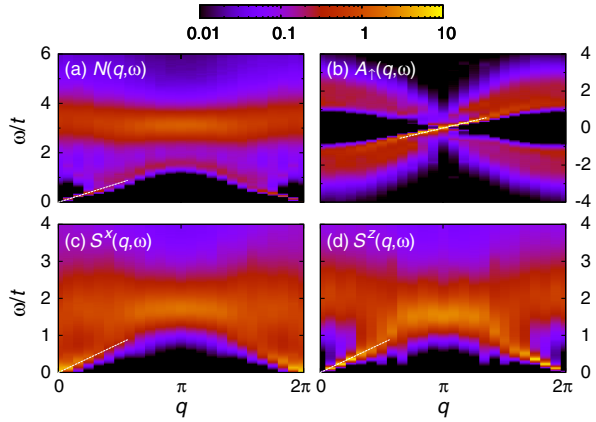

FIG. 5 (color online). Dynamic spectral functions in the (a) charge sector, (b) spin-resolved one-particle sector, and (c), (d) spin sector, measured along the edge. The parameters are $U/t = 2$, $L = 24$, $L' = 64$, $\lambda/t = 0.25$, and $\beta t = 40$. Dotted lines show the velocities of the free helical liquid ($U/t = 0$).

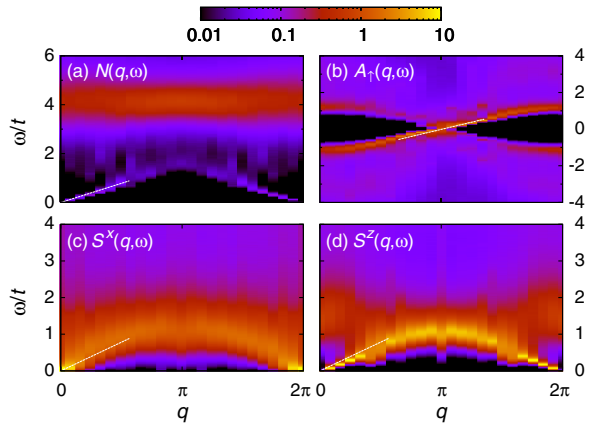

FIG. 6 (color online). Same as in Fig. 5 but for $U/t = 5$.

correlations, the single-particle spectrum [Fig. 6(b)] still exhibits the typical signature of the helical edge state. The growth of the equal-time transverse ferromagnetic correlations as a function of U/t (Fig. 4) leads to a piling up of low-lying spectral weight in $S^x(q, \omega)$ for $q \to 0$.

In the TBI phase, where the effective model of Eq. (3) is valid, one can argue that the charge, longitudinal spin, and Fermi velocities should be rather insensitive to the value of U/t since they are inherited from the bulk. This is confirmed by our numerical results. Correlation effects become manifest in a very strong variation of matrix elements in the dynamic quantities of Eq. (4). In particular, the depletion of low-lying spectral weight in the charge sector suppresses charge transport along the edge. In contrast, spin fluctuations as well as the signatures of the helical liquid in the single-particle spectra persist.

Summary.—We have derived the bulk phase diagram of the Kane-Mele Hubbard model from QMC simulations. We established the exact location of the previously predicted magnetic transition at large U/t [15], and that the nonmagnetic region is dominated by the TBI. The single-particle gap provides strong evidence for a quantum phase transition at finite SO coupling between the QSL and the TBI. Neither of these states can be characterized by a local order parameter, and a detailed understanding of the transition represents a fascinating open issue. Applying the QMC method to an effective model of the helical edge states, we have studied the impact of electronic correlations by calculating one- and two-particle dynamics in the TBI phase. Correlation effects lead to an order of magnitude reduction of low-lying long wavelength charge fluctuations, and thereby charge transport, and promote transverse magnetic fluctuations. The single-particle spectrum retains its weak-coupling features.

We particularly thank Z. Y. Meng, A. Muramatsu, and S. Wessel for helpful discussions. We acknowledge conversations with C. Xu, M. Imada, and Y. Yamaji and support from DFG Grants No. AS120/4-3 (T. C. L.) and No. FOR1162 (M. H.) and NSF Grant No. PHY05-51164 (T. C. L., F. F. A.). We thank the LRZ Munich and the Jülich Supercomputing Centre for generous allocation of CPU time.

Note added.—After completion of this work, a QMC investigation [23] and two approximate studies [24,25] of the same model came out.

[1] M. Z. Hasan and C. L. Kane, Rev. Mod. Phys. **82**, 3045 (2010).
[2] C. L. Kane and E. J. Mele, Phys. Rev. Lett. **95**, 226801 (2005).
[3] F. D. M. Haldane, Phys. Rev. Lett. **61**, 2015 (1988).
[4] C. Wu, B. A. Bernevig, and S.-C. Zhang, Phys. Rev. Lett. **96**, 106401 (2006).
[5] C. Xu and J. E. Moore, Phys. Rev. B **73**, 045322 (2006).
[6] M. König *et al.*, Science **318**, 766 (2007).
[7] D. Hsieh *et al.*, Nature (London) **460**, 1101 (2009).
[8] S. Raghu, X. L. Qi, C. Honerkamp, and S. C. Zhang, Phys. Rev. Lett. **100**, 156401 (2008).
[9] K. Sun, H. Yao, E. Fradkin, and S. A. Kivelson, Phys. Rev. Lett. **103**, 046811 (2009).
[10] Y. Zhang, Y. Ran, and A. Vishwanath, Phys. Rev. B **79**, 245331 (2009).
[11] J. Wen, A. Rüegg, C. C. Joseph Wang, and G. A. Fiete, Phys. Rev. B **82**, 075125 (2010).
[12] M. Dzero, K. Sun, V. Galitski, and P. Coleman, Phys. Rev. Lett. **104**, 106408 (2010).
[13] D. Pesin and L. Balents, Nature Phys. **6**, 376 (2010).
[14] C. N. Varney, K. Sun, M. Rigol, and V. Galitski, Phys. Rev. B **82**, 115125 (2010).
[15] S. Rachel and K. Le Hur, Phys. Rev. B **82**, 075106 (2010).
[16] D. Soriano and J. Fernández-Rossier, Phys. Rev. B **82**, 161302 (2010).
[17] J. Goryo and N. Maeda, arXiv:1007.4671v2.
[18] Z. Y. Meng *et al.*, Nature (London) **464**, 847 (2010).
[19] F. F. Assaad and H. G. Evertz, Lect. Notes Phys. **739**, 277 (2008).
[20] Transitions between trivial and topological band insulators can only occur via a metallic state.
[21] A. N. Rubtsov, V. V. Savkin, and A. I. Lichtenstein, Phys. Rev. B **72**, 035122 (2005).
[22] D. J. Luitz and F. F. Assaad, Phys. Rev. B **81**, 024509 (2010); F. F. Assaad and T. C. Lang, Phys. Rev. B **76**, 035116 (2007).
[23] D. Zheng, C. Wu, and G.-M. Zhang, arXiv:1011.5858v1.
[24] Y. Yamaji and M. Imada, arXiv:1012.2637v1.
[25] S.-L. Yu, X. C. Xie, and J.-X. Li, arXiv:1101.0911v1.